

# A 36 cm<sup>2</sup> Large Monolithic pn-CCD X-ray Detector for the European XMM Satellite Mission

L. Strüder, H. Bräuninger, U. Briel, R. Hartmann, G. Hartner, D. Hauff, N. Krause, B. Maier,  
N. Meidinger, E. Pfeffermann, M. Popp, C. Reppin, R. Richter, D. Stötter, J. Trümper and U. Weber  
*MPI für extraterrestrische Physik, Halbleiterlabor,  
Paul-Gerhardt-Allee 42, D - 81245 München*

P. Holl, J. Kemmer, H. Soltau, A. Viehl and C.v. Zanthier  
*KETEK GmbH, Am Isarbach 30, D - 85764 Oberschleißheim*

## 1 Abstract

Monolithic arrays of 12 pn-CCDs,  $3 \times 1$  cm<sup>2</sup> each, have been developed and produced for the focal plane instrumentation of the high throughput European Photon Imaging Camera (EPIC) on XMM and the German ABRIXAS X-ray satellite mission. The design parameters have been optimized to match the properties of the X-ray imaging optics as well as the X-ray intensity, energy bandwidth and characteristic time constants of objects to be observed.

The pixel size is  $150 \times 150$   $\mu\text{m}^2$ ; read-out is performed in parallel with 64 channels in each subunit, resulting in a total of 768 channels; low noise, spectroscopic performance is realized by on-chip integrated JFET electronics; highohmic, ultrapure bulk material allows full depletion and enhances the efficiency for higher energy X-ray detection. The fabrication process, the layout topology and the operating conditions guarantee for a ten years operation in space without performance degradation.

## 2 Basic Concept

The pn-CCD detector system has been designed for the European X-Ray Multi Mirror satellite mission (XMM) which is planned to be launched in 1999. The basic concept and layout of the detector as well as measured results are found in references [1,2]. Fig. 3 shows the layout of the focal plane. The sensitive area of the detector consists of a  $6 \times 6$  cm<sup>2</sup> large array of 12 pn-CCD units monolithically integrated on a 4 inch wafer. Fig. 1 gives a schematic cross section through the pn-CCD along a transfer channel. In Fig. 2, one functional element of the 36 cm<sup>2</sup> large sensor, a  $3 \times 1$  cm<sup>2</sup> large pn-CCD subunit is shown. Each CCD subunit is 200 pixels deep and 64 pixels wide. The pixel size of  $150 \times 150$   $\mu\text{m}^2$  is matched to the angular resolution of the XMM telescope, which yields a half energy width (HEW) of about  $500 \mu\text{m}$  (corresponding to 15 arcsec). The pn-CCD is a fully depleted silicon radiation detector [3] which is sensitive over the whole wafer thickness of  $280 \mu\text{m}$ . It is illuminated from the rear side, formed by an ultrathin reverse biased pn-junction. The signal electrons are drifting within about 1 ns in a small cloud towards the transfer channel about  $15 \mu\text{m}$  below the register surface. As shown in Fig. 2 each transfer channel is terminated by an anode and an integrated first amplifying stage which consists of a single sided gate JFET. From there the 64 signals of each row are fed in parallel to the CAMEX64B chip [1] for amplification, shaping, sampling and multiplexing. The CAMEX output is sent to a 12-bit 10MHz ADC. The pn-CCD camera has a size of 36 cm<sup>2</sup>, with  $150 \times 150$   $\mu\text{m}^2$  pixel size and a format of  $400 \times 384$  pixels on  $280 \mu\text{m}$  fully depleted high resistivity n-type silicon and is being read out in 4.5 ms.

## 3 Performance Parameter

Extended measurements have been performed at the X-ray test facilities of the Max-Planck-Institut für extraterrestrische Physik. Some relevant measurement results reflecting the state of the art of the chip quality and recent improvements are briefly summarized. All measurements have been made in a single photon counting mode, except the quantum efficiency in the visible spectrum and the DC measurement at the synchrotron. All measurements were performed at temperatures between 140 K and 160 K, except the measurement of the UV, visible and infrared light.

### Electronic and System Noise, Dark Current

The equivalent noise charge of the pn-CCD system is  $4\text{-}5 e^-$  rms for an integration time of 100 ms and an equivalent readout time of 350 ns per pixel. The noise shows negligible temperature dependence between 120 K and 190 K. The dark current contribution is small despite a sensitive thickness of  $280 \mu\text{m}$ . The largest noise contribution still arises from the on-chip JFETs noise, cross talk and electronic pick up. The readout speed is not limited by the electronic noise or transfer properties, but only by the total power dissipation of the focal plane, which should not exceed 0.7 W.

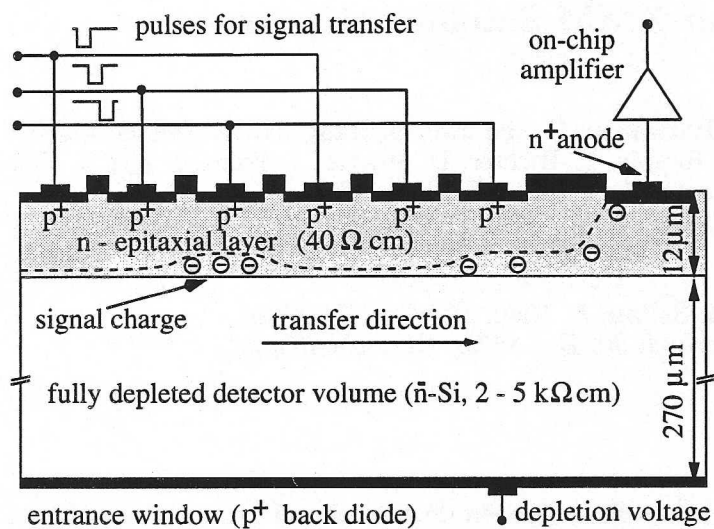


Figure 1: A schematic cross section through the pn-CCD along a transfer channel. The device is back illuminated.

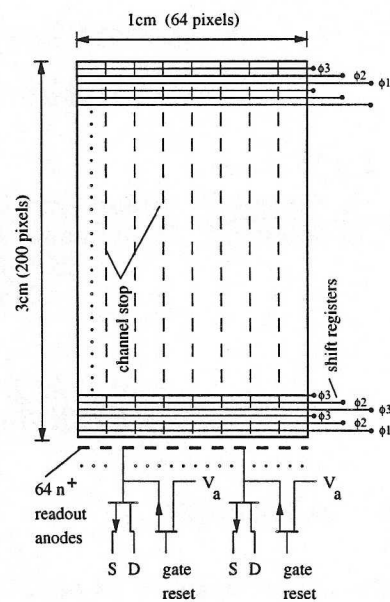


Figure 2: One pn-CCD subunit with 64 on-chip amplifiers and a size of  $3 \times 1 \text{ cm}^2$ .

### Spatial Uniformity

The spatial uniformity in the CCDs electrical performance is excellent. The recent fabrications created a large number of wafers with homogenous noise distribution and uniform spectroscopic behaviour. Only a small number of single defects ( about 1 defect per chip ) occurred. In the PANTER test facility, where the X-ray source is operated 130 m far from the pn-CCD, a flat field illumination was made with  $\text{Ti}_{L\alpha}$  ( $E = 452 \text{ eV}$ ). The spatial homogeneity of the response was better than 1%. The measurement precision was limited by the statistics. Operated in a single photon counting mode each individual pixel was exposed to approximately 20 photons. The photon rate per readout frame was lower than 100, the frame rate was 12 per second.

### Charge Transfer Efficiency

The charge transfer efficiency of the pn-CCD is good. Fig. 4 shows the scatter plot of an  $^{55}\text{Fe}$  source: the charge loss between the first and the last pixel of the CCD is almost negligible. However, a certain dependence of the charge loss on temperature and emission rate is still observed. The effect is dedicated to electron traps with energy levels at about  $-0.3 \text{ eV}$  below the conduction band edge [4]. To minimize the effect of the trap levels the design of the transfer channel and the operation parameters have been changed: the signal electrons are now transferred from the last to the first row in a  $8 \mu\text{m}$  narrow notch within  $4.5 \text{ ms}$ . At 145 K the charge loss over a distance of 3 cm is roughly 1%. At room temperature the transfer loss over the same distance is smaller the 0.1%.

Ionizing radiation causes damage at the  $\text{SiO}_2 - \text{Si}$  interface and lattice defects all over the silicon bulk. Against the surface damage the pn-CCDs are protected because of the use of JFET instead of MOS technology. Concerning the bulk damage the spatial confinement of the signal charges is essential; The pixel volume is reduced as much as possible. In addition, the fringing fields deep in the channel help to transfer a detrapped charge back in the pixel carrying the signal electrons. We have tested the degradation of the pn-CCDs with an equivalent radiation dose of a 10 years mission ( $3.5 \times 10^8$  protons of 10 MeV) and have observed a 5 eV degradation of the energy resolution. The devices were also exposed to alpha particle and gamma ray damage, without significant consequences.

### Entrance Window, Low Energy Performance

The pn-CCD has the advantage to be illuminated from its rear surface, yielding a homogenous entrance window for all incoming photons. The absence of silicon oxide, silicon nitride and polysilicon in the radiation entrance window is essential for low photon energies. For the pn-CCD this results in good spectroscopic performance and high quantum efficiency (see Fig. 5 and 6). The quantum efficiency is higher than 80% for carbon K ( $E = 282 \text{ eV}$ ) and 85% for oxygen K ( $E = 523 \text{ eV}$ ), conserving the good spectroscopic performance (see Fig. 8). As the whole wafer volume is depleted the quantum efficiency is high even for high photon energies, e.g. 91% at 10 keV. However a certain reduction of the energy resolution is observed at low energies: as the absorption length is decreasing the influence of the properties of the entrance window is growing.

The peak-to-valley ratio in Fig. 7 accounts to 6000:1 for  $^{55}\text{Fe}$  ( $E = 5898 \text{ eV}$  and  $6490 \text{ eV}$ ) and to 2000:1 for aluminum X-rays ( $E = 1487 \text{ eV}$ ).

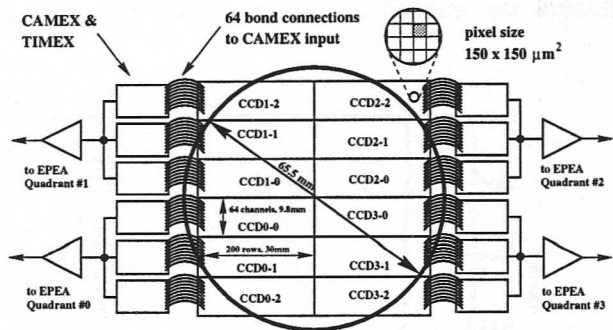


Figure 3: The pn-CCD focal plane area as designed for XMM. It has a sensitive area of  $36 \text{ cm}^2$ , a total of 768 readout channels, multiplexed with a JFET/CMOS amplifier array at 10 MHz.

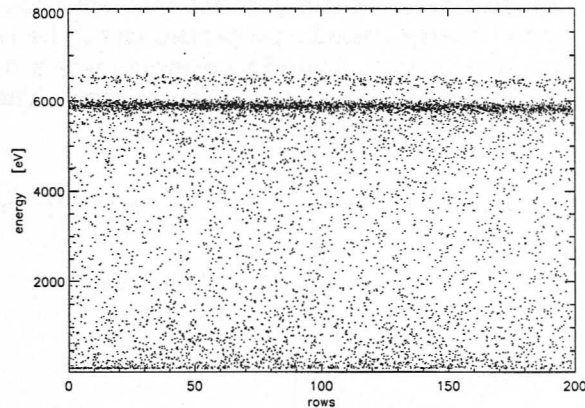


Figure 4: The absolute charge loss of the pn-CCD after a transfer over 3 cm. The photons were generated by an  $^{55}\text{Fe}$  radioactive source ( $E = 5898 \text{ eV}$  and  $6490 \text{ eV}$ ).

Fig.6 shows the measured quantum efficiency from 60 eV up to 9 keV. In this energy range the penetration depth of the radiation varies by 5 orders of magnitude, while the response of the detector only changes by a factor of 2. Most remarkable is the quantum efficiency from the UV light up to the near infrared spectrum as shown in Fig. 5. From 200nm to 900nm the response to photons is about 70%. The sudden increase at 4.5 eV (250 nm) corresponds to the two electron/hole pair creation process. In the lower energetic part of the spectrum only one electron/hole pair per photon is generated. The limitation to 70% is mainly due to reflection of the incident radiation at the silicon surface.

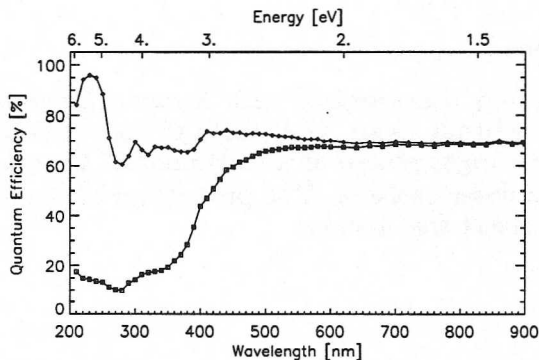


Figure 5: Sensitivity of pn-CCDs from the UV light to the infrared light at 900 nm. The increase at 4.5 eV is due to the creation of two electron/hole pairs by one photon.

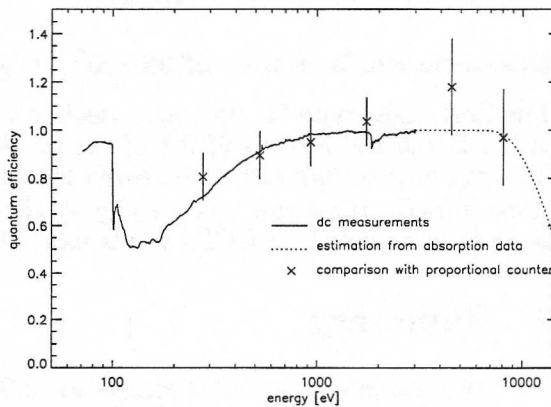


Figure 6: Quantum efficiency measured in a dc photocurrent mode (solid line) and in a single photon counting mode (+ signs). The dotted line is the QE calculated from the photon absorption coefficients

### Space, Time and Energy Resolution

The space resolution is  $130 \times 130 \mu\text{m}^2$ , determined by the pixel size of  $150 \times 150 \mu\text{m}^2$  and the average size of the electron cloud in the transfer region of about  $20 \mu\text{m}$  diameter.

The time resolution can be varied between  $50 \mu\text{s}$  and  $1000 \mu\text{s}$  (timing mode) and  $50 \text{ ms}$  to  $500 \text{ ms}$  (full frame mode). In the full frame mode, which is the standard timing, a minimum integration time of  $45 \text{ ms}$  is followed by a read-out cycle of about  $4.5 \text{ ms}$ . In the timing mode the charge collected in each single row is summed in blocks of 10 rows losing spatial and gaining time resolution.

Fig. 7 shows a manganese-K-spectrum ( $E = 5898 \text{ eV}$  and  $6490 \text{ eV}$ ) with energy resolutions of  $130 \text{ eV}$  and  $135 \text{ eV}$  respectively. The FWHM of the  $\text{K}_\alpha$  X-rays of carbon ( $E = 282 \text{ eV}$ ) and oxygen ( $E = 523 \text{ eV}$ ) line amounts to  $75 \text{ eV}$ , as can be seen in Fig. 8. For low energy X-rays, the system energy resolution is first of all determined by the electronic noise and the dark current. The Fano noise is

the dominant contribution for high energies. The charge transfer noise due to statistical fluctuations in the charge transfer properties has to be added as a function of temperature, timing, X-ray energy and photon rate. Out of time events which reach the detector during the read-out-cycle reduce mainly the position resolution of the detector. They influence the energy resolution in the case of a poor charge-transfer-efficiency.

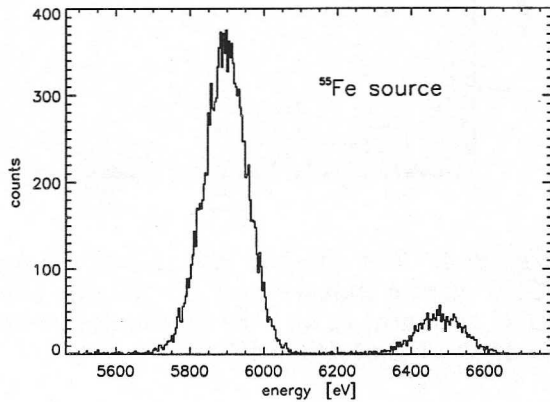


Figure 7: *Manganese spectrum in a flat field measurement at a readout speed of 4 ms for a  $3 \times 1 \text{ cm}^2$  large pn-CCD detector. The FWHM of the Mn  $K_{\alpha}$  peak is 130 eV only.*

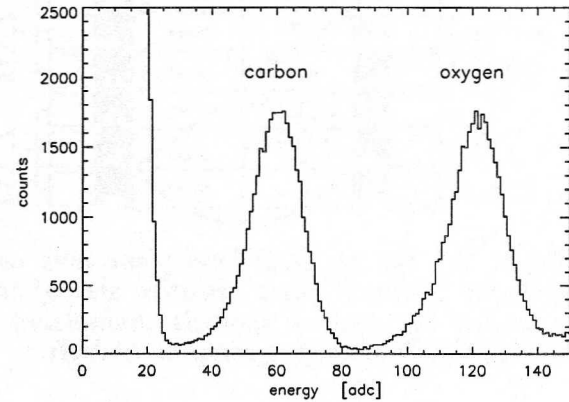


Figure 8: *Carbon ( $E = 282 \text{ eV}$ ) and oxygen ( $E = 523 \text{ eV}$ ) spectrum in a single photon counting mode. The FWHM is about 75 eV for both lines and the QE is above 85%.*

The effect of charge splitting is less pronounced for the pn-CCD as for MOS-CCDs due to the comparable large pixel size and the strong drift field over the whole detection depth. A percentage as high as 75 of the photon events shows up as single events, only 2 % split in three or four pixels. Summation of the split events is possible with good success. The energy resolution of the single event spectra is affected by charge splitting in those cases where the charge deposited in the neighbouring pixel remains under the event threshold.

#### Cosmetic Performance of $36 \text{ cm}^2$ Large Devices

The first flight type  $36 \text{ cm}^2$  large devices have been fully characterized with X-rays. For about 10% of the fabricated devices 99.9% of the pixels are cosmetically clean. Only 0.1% of the pixels over the full area have shown either increased leakage current (bright pixels) or a bad transfer. In some cases these imperfections can be optically localized on the wafer surfaces. The production of the  $3 \times 1 \text{ cm}^2$  large fully depleted pn-CCDs yields more than 90% defect free devices.

## 4 Summary

We have designed, fabricated and tested a  $36 \text{ cm}^2$  large X-ray pn-CCD array, depleted over the whole wafer thickness ( $280 \mu\text{m}$ ), for the European XMM and the German ABRIXAS satellite mission. Its response to radiation is higher than 90% from 500 eV up to 10 keV. In the visible domain the efficiency is almost constant at 70% from 200 nm to 950 nm. The electronic system noise is below 5 electrons rms. The charge transfer properties are good at low temperatures as well as at room temperature. Maintaining the above properties of the pn-CCD system, the pixel size can be reduced to  $30 \times 30 \mu\text{m}^2$  or extended to  $500 \times 500 \mu\text{m}^2$ . For small pixel sizes, this leads to an X-ray position resolution of 2 - 5  $\mu\text{m}$ , if the center of mass of the charge cloud in the pixels is determined.

*The project was supported by the Deutsche Agentur für Raumfahrtangelegenheiten (DARA) under contract No. 50 OX 93025/-XMM-EPIC.*

## 5 References

- [1] L. Strüder et al., Nucl. Inst. Meth. A253, pp 386 - 392, (1987)
- [2] H. Soltau et al., Nucl. Inst. Meth. A377, pp 340 - 346, (1996)
- [3] N. Meidinger et al., SPIE Vol. 2808, pp 492 - 504, (1996)
- [4] N. Meidinger et al., Nucl. Inst. Meth. A377, pp 298 - 311, (1996)
- [5] R. Hartmann et al., Nucl. Inst. Meth. A387, pp 250- 254, (1997)